2.4. ASSESSMENT OF CORIUM STABILISATION

2.4.1. Principal strategy

To stabilize the molten core in a severe accident, the EPR relies on an ex-vessel strategy based on the provision of a dedicated water-cooled core catcher. In-vessel melt retention by outside cooling was dismissed because of the high power rating of the reactor and the related low margins for heat transfer. The EPR core catcher into which the melt spreads has a large surface, which increases the surface-to-volume ratio and makes the subsequent cooling of the melt effective.

The core catcher is located in a dedicated compartment lateral to the pit. The connection between pit and spreading compartment is normally closed. In a severe accident the separating plug will be opened by the melt itself. Thanks to the related spatial separation, the core-catcher in the spreading room is safe from potentially critical loads related to the failure of the reactor pressure vessel (RPV). Conversely, unintentional flooding of the core catcher during power operation does not affect the safety of the plant. As a consequence of this uncoupling of the provisions for severe accident mitigation from operational components and systems, power operation and design-basis accident mitigation measures remain unaffected by the existence of the core catcher.

To promote spreading of the melt into the core catcher, the EPR concept involves a phase of temporary melt retention in the reactor pit. This measure responds to the prediction that the release of the molten material from the RPV is not likely to take place in a single pour, but will occur in a discontinuous manner. Temporary retention is based on the provision of a layer of sacrificial concrete that must be penetrated by the melt before it can flow from the pit. The time delay and the admixture of sacrificial concrete results in a more uniform spectrum of possible melt states at the end of the retention process. This makes the spreading process and all subsequent stabilization measures largely independent of inherent uncertainties associated with in-vessel melt pool formation and RPV failure.

Stabilisation of the spread melt in the metallic core catcher is achieved by means of flooding and external cooling. Interaction with the structural concrete is avoided together with:

- weakening of load-bearing structures and a penetration of the embedded liner,
- long-term heat-up and mechanical deformation of foundation raft and containment building,
- sustained generation of non-condensable gas.

The cooling of the melt spread in the core catcher by the overflow of water from the IRWST is fully passive. Alternatively, the containment heat removal system (CHRS) can be used to actively deliver cooling water to the cooling structure. In this case, steaming into the containment will be terminated resulting in the establishment of long term atmospheric pressure conditions inside the containment,

The EPR melt stabilization concept involves the following sequence of events (see S.2.2.4 FIG 1):

- failure of the RPV and the subsequent release of the molten core
- temporary retention of the released material in the pit
- opening of the gate and the relocation of the accumulated melt into the core catcher
- passive flooding and quenching of the spread melt
- long term cooling and heat removal

By this sequence an automatic and fully passive transformation of the molten corium into a coolable configuration is achieved on the basis of simple physics and without requiring operator action or active internal or external systems.

The above stages, and related main components and principles of operation, are described in detail in the following.

2.4.1.1. Melt Release from the reactor pressure vessel

Core melting starts after all emergency measures have failed to maintain the core in a coolable and cooled configuration. The course of the subsequent destruction and melting of the core depends on the related accident scenario and on the initial state of the core. Both involve a significant degree of uncertainty.

The heavy reflector of the EPR influences the melt down process in a way that it spatially constrains the melt and leads to the formation of a temporary mainly oxidic molten pool on top of the lower support plate. The heat transport within this pool will be driven by natural circulation. Therefore, even without a metal layer on top, the heat flux to the vessel side will be much higher than to the bottom and it is therefore expected that the melt will penetrate the heavy reflector at the side before the failure of the lower support plate.

A sideways penetration is in accord with theoretical predictions and with the results of experiments, (see for example the SULTAN [20], COPO [21], FOREVER [22] programmes). Following a sideways failure, the entire upper part of the molten pool will relocate into the lower head. Subsequent discharges will be more gradual and will be influences by the progressive destruction of the core, and the widening of the failure site by the continuing outflow of melt.

After relocation into the lower head, the decay-heated melt/debris will first be quenched by residual water and then will reheat to form a second molten pool. According to the results of the MVI project [1], the resulting RPV failure is expected to be localised and – for vessels without penetrations in the lower head - to occur at an elevation near the interface between the molten oxide and metal layers. Such a failure will result in the outflow into the pit of all melt above the hole.

At the time when the MCCI begins to take place in the pit, melt/debris may still be present in the RPV between the lower head and the coresupport plate. The continuing release of decay heat will lead to a steady heat-up of this material and other in-vessel structures, resulting in further melting. In addition to the heat-up from the inside, the bottom of the lower head is exposed to thermal radiation from the surface of the MCCI pool. The in-vessel phase ends after creep-failure of the lower RPV. The detached structure, plus the remaining debris, will then be incorporated into the MCCI pool.

2.4.1.2. Temporary retention in the reactor pit

2.4.1.2.1. Description of the chosen strategy

The initial conditions for melt stabilization are determined by the actual scenario, the course of in-vessel core degradation, relocation and quenching, and finally by the sequence of melt release after failure of the lower head. All these processes naturally involve a significant degree of uncertainty and unpredictability. To make the EPR melt stabilization concept tolerant to these uncertainties, the concept involves engineering a phase of temporary melt retention and accumulation in the reactor pit. Without retention, this release could result in undefined and potentially unfavourable conditions for the relocation of the melt in the lateral core catcher.

Temporary retention results in a "spreading in a single event" and is based on the provision of a layer of sacrificial material that must be penetrated by the melt prior to it being allowed to escape from the pit. The corresponding delay ensures that, even in case of an incomplete first release of melt from the RPV, practically the entire core inventory will be collected in the pit (if it is not otherwise re-stabilized).

The reactor pit is designed to withstand the loads resulting from a failure of the RPV under an internal pressure of 20 bar. The related loads include melt jets and the potential mechanical impact of the detached lower head. The latter is absorbed by dedicated concrete structures, located around the centre of the pit, which also protect the melt plug at the entrance of the transfer channel between pit and spreading compartment (see S.2.2.4 FIG 1).

The sacrificial concrete layer is backed-up by dedicated shielding (see S.2.2.4 FIG 1); the latter confines the melt and protects the RPV support structure from the melt in case of a local penetration of the sacrificial concrete. The layer consists of zirconia-based refractory material. Its thermal-mechanical stability against an attack of the metallic and oxidic melt fraction has been proven under prototypic conditions by dedicated experiments [2].

The provision of a layer of sacrificial concrete of defined thickness has a favourable self-adjusting characteristic. This stems from the fact that, to ablate a fixed amount of concrete, the melt must generate a fixed amount of decay heat. Therefore, a lower initial mass of released melt and/or a lower level of decay heat both result in correspondingly longer retention times, and vice versa.

This independence is further reinforced by the fact that the RPV, the melting core, the MCCI pool, and the sacrificial concrete form a coupled adiabatic system. The residual RPV is not only heated from the inside, but also from the outside by thermal radiation from the surface of the MCCI[1] pool. The corresponding radiant heat flux is always of the same order as that into the surrounding concrete, due to effective gas-induced mixing within the MCCI pool. Therefore, the progress of concrete ablation is necessarily linked with the heat-up and thermal failure of the RPV.

Both, the fixed position of the gate and the geometrical constraint imposed by the refractory layer, pre-determine the total amount of concrete ablated during the retention period. This forces the final melt properties, which mainly depend on the concrete fraction, into a narrow and well-defined range. The temperature of the final melt will be several hundred degrees above its immobilization temperature, which ensures a low viscosity and is highly favourable for melt spreading.

The characteristics of the retention period, and the consequential equalization of the spectrum of possible melt states at the end of the retention process, make the spreading process and all subsequent measures independent of the inherent uncertainties associated with in-vessel melt pool formation and RPV failure.

[1] MCCI: Molten Core Concrete interaction

2.4.1.2.2. Selection of sacrificial materials for the reactor pit

The composition of the sacrificial concrete employed in the reactor pit is specifically selected to meet the requirements of the temporary melt retention. The concrete aggregates dominantly consist of Fe_2O_3 and SiO_2 in approximately equal proportion, while 15 wt% of common Portland cement in the dry concrete mixture is used as a binder.

Fe_2O_3 favourably contributes to oxidizing the chemically aggressive metals Zr and U. The reaction by-product Fe does not affect the thermo-chemical characteristics of the melt. In addition, after the dissolved metal inventory in the oxide depletes, surplus Fe_2O_3 accumulates as FeO and Fe_3O_3 in the oxide melt, thus reducing the liquidus temperature and correspondingly, the temperature level at which the MCCI takes place. This effect is beneficial as, in combination with the formation of silicates, it contributes to reducing the fission product release from the MCCI pool.

Fe_2O_3 and SiO_2 are provided in their natural modification form as iron ore and siliceous pebble. Therefore, $MgCO_3$ (dolomite) and $CaCO_3$ (limestone) are additionally introduced into the concrete system. The concrete was found to have similar mechanical characteristics as ordinary concrete and a water content of less than 5wt% after a drying period of 150 days.

2.4.1.2.3. Consequences of postulated late reflooding

If, after the start of core melting, water will be introduced into the RPV through the primary circuit, either by passive or active means, a part of the core may become temporarily or permanently quenched and re-stabilized. The effectiveness of this process depends on the status of accident progression and of the question whether or not the RPV has already failed at the bottom.

Reflood before RPV failure

If the RPV is still intact, cooling can potentially lead to a stabilization of the degraded core inside the RPV. If core degradation is in a late state and local molten pools exist, either atop the lower support plate or within the lower head, a stabilization can be impossible once certain configurations are reached and critical pool depths values exceeded.

Water addition and the subsequent quenching and steam production can raise the pressure level in the primary circuit. RPV failure at an elevated internal pressure may then result in: pressure and loads on the walls of the pit as well as impact loads and melt jets. In addition, some of the released melt can become dispersed and carried out of the pit with the steam flow.

Melt jets, could impact the residual concrete cover of the gate. However, for the EPR the formation of small holes in the RPV bottom can be excluded due to the absence of penetrations in the lower head. If a penetration would take place at the bottom due to the attack by a molten pool, the resulting failure cross-section will be large which eliminates the risk of focussed jets.

For gravity-driven outflows of melt with typical velocities of some m/s the erosive effect is negligible, as demonstrated e.g. in the COMET experiments [24] where even flows of superheated metal impacting on concrete from an elevation of several meters, did never cause a significant local erosion. This high resistance is attributed to the fact that the decomposition of concrete creates a large amount of gas, which counteracts the flow of melt and by creating a kind of protective cushion at the location of impact. The possible extent of concrete erosion during a postulated melt outflow in the lower region of the RPV is further limited by the fact that the already released melt will accumulate at the deepest location - that is, atop the gate - which will increasingly disperse the impacting flow.

The extent of melt dispersal after vessel break at low pressure (<2 MPa) have been extensively investigated in an EPR-type geometry in the DISCO experiments at FZK [25]. Tests were performed for central and lateral holes in the calotte of the RPV as well as for a complete unzipping of the lower head.

The results of the tests give information on the flow regimes and the dispersal for the different configurations. Great differences were observed between the results obtained for different corium simulants. For the expected lateral holes a considerable reduction of the dispersal rate was found as compared to central holes. In case of metal as simulant dispersal rate was <10%. The hot tests showed that even for central holes practically no melt was carried into the containment dome. Based on the experimental results the developed codes and correlations predict a dispersed melt fraction of typically < 5% in the real EPR geometry. This low value results from the fact that there is no direct path from the pit into the containment dome.

In the performed containment analysis, a dispersed melt fraction of 10% of the initial mass of 150 t of molten corium was conservatively assumed. The resulting increase in containment pressure caused from direct heat transfer to the atmosphere and combustion of the additionally generated hydrogen remains below 0.1 MPa. The dispersed material is generally fine-fragmented and will be coolable after deposition.

In the wall of the pit, above the level of the protective layer, there are a number of ventilation outlet nozzles that are connected to a pressure resistant cylindrical distribution channel located outside the pit. The nozzles serve to cool the concrete walls of the pit. Under the conditions of a failure of the RPV under elevated pressure, a fraction of the dispersed melt could theoretically enter the ventilation duct. However, the results of the DISCO-experiments [25] demonstrated that the total amount of melt that can enter these channels is negligibly small.

Reflood after RPV failure

If, at the time of reflood, the RPV lower head has already been penetrated by the melt, the water will also fill the pit and consequently also cool the outside of the RPV. In addition, as the heavy reflector was necessarily penetrated before RPV failure, only shallow melt pools can exist on both heavy reflector and within the lower head. Under these conditions, late water addition can be expected to quench, arrest, and cool all material still present inside the residual RPV at the time of flooding.

As a consequence, principally the same final situation will exist, for the two postulated reflood cases, before and after lower head failure. It is characterized by some unknown fraction of the core remaining in-vessel in a stable configuration and the rest being incorporated in the MCCI pool in the pit. The retention concept must ensure that the MCCI pool in the pit, if it is not quenched and arrested there, will finally relocate into the core catcher.

This target is achieved by the chosen strategy to apply sacrificial concrete in the pit combined with by the possibility to flood the pit after gate opening using the CHRS. As theoretically predicted and experimentally confirmed, e.g. in the MACE experiments [3], the characteristics of an MCCI do not depend on whether its upper surface is flooded or not. This is due to the fact that the upward heat flux is mainly determined by the intensity of convection within the molten pool, which is only determined by the masses and geometries involved. What will be influenced though, are the conditions at the interface, where crusts can form in case of a water overlayer, while a dry pool surface remains liquid.

During retention, the MCCI pool will be either mixed or stratified.

In case of a stratified pool the specifically heavier oxidic corium will initially be at the bottom, below the metal layer. As the result of the interaction between metal layer and the concrete of the sidewall, a light slag layer will accumulate atop the metal melt. It predominantly consists of concrete decomposition products, mainly SiO_2, which is rather viscose during cool-down.

In case of a mixed pool, all concrete slag will immediately be dissolved within the oxidic melt, with similar consequences on its viscosity.

Therefore, during flooding, a solidifying glassy oxidic layer can be expected which isolates the MCCI pool below from the water above. As observed in all MACE-tests [3], fuel coolant interactions are safely suppressed under these conditions.

To summarize: flooding can be expected to delay concrete erosion, but not to significantly influence the progression of the molten pool towards the gate, and the spreading of the melt. If a molten pool had not yet formed in the pit at the time of reflood, the still coolable debris will become stabilized within the RPV and will remain there, as long as water is provided by either the ECCS or the CHRS. The molten pool underneath the crust will further progress downward, reach the melt gate, and finally relocate into the core catcher, in the same way as in the dry pit case.

2.4.1.3. Gate opening and melt spreading

The melt plug in the centre of the pit bottom is the only place where the sacrificial concrete is not backed by a protective layer. Therefore the melt plug is the predefined weak point of the pit walls.

At the end of the retention phase the progressing melt will therefore penetrate the melt plug and uncover the entrance of the transfer channel. The melt plug has a cross-section of ~2.4 m². It consists of three parts: a 50 cm thick sacrificial concrete cover, a 4 cm thick plate, the so called “gate”, made of an aluminium/magnesium-alloy, and a support structure which keeps the plug in place during normal operation. To allow access to the RPV for external inspection, the plug can be removed through the transfer channel using a dedicated transport system.

The concrete cover of the plug is an integral part of the sacrificial layer in the pit and has the same thickness, (see S.2.2.4 FIG 1). The gate will therefore be reached by the melt when the overall axial erosion approaches the level of 50 cm. Due to the large diameter of the pit, the ablation front is expected to be practically even and the entire surface of the gate uncovered and penetrated within a short period of time.

The gate rests on a steel frame which forms an open mesh. This ensures that the outflow process will not be hampered by the presence of this structure. To make the melt plug removable, the steel frame is locked against a support structure embedded in the sacrificial concrete layer.

The gate material has a low melting point. In addition, it will interact with the oxidic part of the melt in an exothermic, thermitic reaction. Therefore the gate is expected to fail quickly after melt contact. Even if the gate was postulated to not to open, the melt would finally expose the protective layer around the melt plug and destroy the support of the outer frame, which ultimately results in the complete drop-out of the frame, including the still locked-in gate, under the pressure imposed by the melt.

During gate heat-up, the MCCI continues around the exposed area and along the sidewall. The intensity of convection within the molten pool is determined by the mixing provided by concrete decomposition gas. Due to this and to the fact that the gate area is only a small fraction of the total surface of the molten pool, the heat flux into the gate after the phase of initial contact will be imposed by the MCCI. The final thermal destruction of the aluminium gate is unavoidable, because no cooling is provided on the lower side and because the material interacts in an exothermic, thermitic reaction with the iron-oxide containing melt. The rate of melt discharge after opening of the full cross-section of the gate would be in the order of 10 Mg/s.

Spreading distances equal to the dimensions of the EPR core catcher have been observed in experiments with prototypic corium in the frame of the EU-COMAS project [4] already at melt discharge rates of 100 kg/s and less. Such rates correspond to an open outflow cross-section of less than 0.01 m², more than two orders of magnitude below that of the fully open gate. The formation of such small holes in the gate is physically excluded, as the lateral expansion by the erosive effect of the out-flowing melt will widen the hole and provide a minimum cross-section in the order of 0.3 m², independent on the initial size and location of the hole.

After passing through the gate, the melt flows through the transfer channel and finally pours onto the concrete-covered surface of the core catcher. There it will spread under almost dry conditions. This is due to the fact that the spreading compartment is a dead-end room and isolated from the rest of the containment, so there is no possibility of a direct inflow of water from sprays or leaks. Only a limited amount of condensate may form inside the room. Though dry conditions are not required for successful spreading, they make the distribution of the melt more predictable and further reduce the potential for local fuel coolant interactions.

2.4.1.4. Melt flooding, quenching and cooling

The EPR core catcher, into which the melt is relocated after its release from the pit, is a shallow crucible. Its bottom and sidewalls are assembled from a large number of individual elements made of cast iron, connected using a tongue-and-groove technique. Thanks to this flexible connection method, the structure is largely insensitive to thermal expansion and deformation as a result of temperature gradients. To enhance downward heat transfer, the bottom and sidewall elements have integrated fins that form rectangular, horizontal cooling channels.

The sidewall elements are stacked inside vertical beams. A flexible connection is ensured by a similar technique as that used for the bottom plate. The beams are attached to the surrounding concrete walls with a sufficient gap for outside cooling and for the escape of generated steam. The top of the steam vent is protected by a lid-type structure, which prevents the entry of material that could have potentially been splashed by local fuel coolant interactions. The inside of the crucible structure is covered with a layer of concrete.

The arrival of the melt in the core catcher triggers the opening of valves that initiate gravity-driven flow of water from the IRWST into the spreading compartment. The water first fills the central supply duct underneath the core-catcher. From there it enters the horizontal cooling channels and then submerges the space behind the sidewall cooling structure. With the chosen initial flooding rate of about 100 kg/s, the fill-up process takes about 5 minutes, which is longer than the predicted melt release and spreading time.

After filling, water will overflow onto the surface of the melt from the two sides of the sidewall structure that are farthest away from the melt inlet. Water overflow will continue until the hydrostatic pressure levels between IRWST and spreading room are balanced. This equilibrium state will be sustained throughout the remainder of the accident.

In parallel with the inflow of water, the spread melt interacts with the sacrificial concrete at the horizontal and vertical cooling plates. The requirements on the sacrificial concrete in the core catcher are:

- to provide an easily accessible surface
- to delay the contact between melt and cooling structure
- to mechanically protect the structure during melt spreading
- to reduce temperature and density of the melt prior to its contact with the cooling structure
- to promote melt fragmentation at the surface during flooding

All above listed targets can be achieved with standard siliceous concrete.

The presence of the sacrificial concrete, in combination with the high thermal inertia of the massive cast iron cooling structure, ensure - with high margin - that the outside of the core catcher will be flooded early enough and that maximum heat fluxes to the water remain within tolerable limits for all possible melt release scenarios and corresponding melt states.

During MCCI, the temperature and the specific weight of the oxidic melt fraction are steadily reduced by the incorporation of concrete decomposition products. Therefore, the final formation of a density-stratified system with a lighter oxide layer on top of a heavier metal layer is certain even though, during MCCI, a part of the metal could temporarily remain suspended within the oxidic phase. Therefore:

- the water that pours onto the melt will come in contact with the oxidic melt fraction:

  According to the results of the MACE project [3], [9], [12], this can result in substantial superficial fragmentation and improved coolability that would significantly shorten the period of liquid melt states. Further, the formation of an oxidic crust and the avoidance of the contact between metal and water will strongly reduce the probability of a local FCI.

- the cooling structure will most likely first come in contact with the metallic melt fraction:

  Due to the high heat loss during concrete ablation, the temperature of the metal will decrease below its solidification temperature. This leads to the formation of crusts, which reduce the transient thermal loads during the subsequent contact with the cooling plate. For a contact between cooling structure and an oxidic melt these transient loads are much lower, anyway.

The tolerance of the cooling structure against bounding transient loads (see 2.4.3.6.1 within this subchapter) was confirmed experimentally by dedicated tests in a full-scale rectangular horizontal channel [23]. The tests confirmed that the heat transfer to the water is sufficiently effective over the entire range of expected heat fluxes from the melt. This establishes comfortable margins for the cooling of the melt and results in a high tolerance against local deviations in the final melt depth as well as in the absence of restrictions regarding the distribution of the metallic and oxidic phases.

The experimental results further showed that the heat transfer inside the channel is equally effective under both co-current and counter-current flow conditions, which correlates to a passive inflow of water from either the IRWST or the saturated pool atop the melt. This voids the need to sustain defined flow conditions for each individual channel. Instead, it is sufficient to keep the core-catcher submerged. In the EPR design, this is guaranteed by the open connection between the IRWST and the spreading room. Therefore melt cooling is achieved in a fully passive way; no pump and no external water supply are needed.

Further, as the stabilization of the melt is exclusively based on heat transfer and crust formation, there are no limiting thermo-chemical constraints, so there is no need to establish a certain range of melt compositions. This reduces the requirements on preceding measures, namely on temporary melt retention and on the choice of an appropriate type of sacrificial concrete.

2.4.1.5. Long term cooling

In the early phase of flooding, when the surface of the melt is still hot, all added water can be expected to evaporate. Later, a saturated water pool will form atop an evolving crust. This crust will steadily expand from the circumference towards the centre. The steam from the boiling pool merges with the steam resulting from bottom and sidewall cooling. When the core catcher is entirely flooded (see S.2.2.4 FIG 3) and quasi-steady conditions achieved, the amount of steam discharged into the containment corresponds to the total decay power in the melt.

2.4.2. Analysis performed

2.4.2.1. Validation of the temporary retention of the corium in the reactor pit

The temporary melt retention in the reactor pit responds to the prediction that the release of the molten material from the RPV will, most likely, not take place in one pour, but bit by bit. It is based on the provision of a layer of sacrificial concrete that must be penetrated by the melt prior to its escape from the pit.

Deviations from the expected isotropic character of the MCCI can result in a local contact between the melt and the zirconia at a time when the rest of the zirconia is still covered with concrete. Though the analysis of the MCCI in the pit, as presented later in this section, does not account for such irregularities, but yields "averaged" predictions only, the protective material must be sufficiently stable against both the metallic and oxidic melt fraction under the conditions of an ongoing MCCI in the pit. This stability has been experimentally confirmed.

The stability results from the fact that during MCCI there is a permanent introduction of "cold" concrete decomposition products into the bulk of the melt, which leads to the formation of a sub-cooled two-phase mixture. This mixture consists of: (i) a dispersed solid phase that contains mainly high-melting refractory components (zirconia, urania), and (ii) a liquid phase that contains the low melting concrete decomposition products plus the remaining refractory components. As a consequence, the melt is "saturated" in refractory components. As long as the MCCI continues, it will keep the temperature and the properties of the oxidic melt in a range that avoids any significant dissolution of the exposed zirconia.

Besides its main function to accumulate the melt after its release from the RPV, temporary melt retention and the admixture of sacrificial concrete in the pit are intended to equalize the spectrum of possible melt states at the end of the retention process. This is favourable, as it makes the subsequent stabilization measures independent of the inherent uncertainties associated with in-vessel melt pool formation and RPV failure.

This section describes the strategy used to validate melt retention and accumulation in the reactor pit of the EPR as well as the main results obtained.

2.4.2.1.1. Validation strategy

The initial and boundary conditions for this analysis are provided by the characteristics of the preceding melt release after failure of the RPV, which include the discharge sequence into the reactor pit, the masses of oxidic and metallic components involved and their corresponding thermodynamic and thermo-chemical state.

The corresponding data are provided by integral codes, such as MAAP 4. However, as the late in-vessel melt progression is an ongoing R&D issue, the models incorporated in these codes, and correspondingly the obtained predictions involve a significant degree of uncertainty.

Apart from these uncertainties, the feedback of thermal radiation emitted between the MCCI pool in the pit and the RPV lower head, which for EPR conditions, can significantly influence the time of complete lower head failure, is not adequately reflected in these codes. Therefore, the validation of the accumulation function of the pit is performed on the basis of generalized melt release sequences, using integral considerations. Nevertheless, the modelling of these sequences still rests on predictions of the plant state and the amount of melt obtained from integral codes.

The advantage of the chosen strategy is that the validation of the design becomes independent of the spectrum of scenarios and of the variability of melt release modes.

Apart from the representative release sequences in which a significant fraction of the melt consists of oxide, a bounding sequence in which the initial pour consists largely of metallic melt is considered. This is because such a release has the potential to prematurely fail the melt plug due to the high rate of transient concrete ablation. Accordingly, the validation strategy addresses this issue using a bounding assumption that the first pour consists exclusively of metallic melt.

The generalized melt release sequence is based on the modelling scheme sketched in S.2.2.4 FIG 2.

As the core of the EPR is enclosed by a heavy reflector, it is assumed that a molten pool forms on the lower support plate before significant attack and melt-through of the heavy reflector takes place. At some time this pool starts to discharge into the lower head, while new material is added from the core above. Ultimately two partially molten pools will coexist, one located in the lower head, the other above the core support plate, see S.2.2.4 FIG 2a.

The prediction of the amount of melt in the lower head that can initially be released into the pit after local failure of the RPV involves significant uncertainties. The approach followed here is to envelop these uncertainties by a parametric variation of the amount of melt that is initially released in the pit, and by considering the feedback between melt concrete interaction in the pit and RPV heat-up and failure. This involves the assumption of various initial melt masses with correspondingly different surface/volume ratios initially released into the pit.

Due to the effective coupling by radiant heat transfer between lower head and lower support plate, see S.2.2.4 FIG 2b, the melt residing in these regions is concentrated into a single equivalent mass, thereafter called RPV-bottom, see S.2.2.4 FIG 2c. The RPV-bottom is assumed to be heated by thermal radiation emitted from the MCCI pool in the pit and by a fraction of the decay heat generated in the molten pool atop the lower support plate.

The RPV-bottom is assumed to fail as soon as it reaches a given failure temperature. Upon failure, the fraction of the oxidic and metallic melt which is still in the vessel is discharged into the reactor pit. Also, the RPV-bottom adds to the MCCI pool. The temperature at which ultimate lower head failure takes place is taken as the temperature at which the ultimate strength of the steel is practically zero. High temperature tensile data for RPV steel indicate that this will occur at about 1300 °C. Likely, the lower head would already fail at temperatures below this level due to the significant creep, which results in a steady reduction of the load-bearing cross-section.

As a consequence, the selected generalized melt release sequence involves two distinct melt pours. While the first pour initiates the MCCI, the second, which comprises the residual in-vessel melt inventory, practically terminates the melt release from the RPV. In reality, other melt discharge sequences are also conceivable. These are addressed by varying the initially released melt fraction from 40% to 80% of the total oxidic and metallic melt inventory.

The metallic and oxidic melt masses and compositions constitute an upper bound for the melt masses predicted by MAAP for various scenarios. The in-vessel Zr-oxidation level was assumed to be 40%. Due to the good solubility of Zr [9], almost the entire Zr-inventory is assumed to be dissolved in the oxidic melt fraction with only a small portion of Zr in the metallic melt.

The initial temperature of the oxidic melt is assumed to be the liquidus temperature for the given composition. This assumption constitutes the upper bound of the range predicted by MAAP 4 and is conservative with respect to the energy content in the melt. A higher energy content translates into higher ablation rates and hence, reduced retention times. The initial temperature of the metallic melt is assumed to be 1550°C, which is representative of the temperatures predicted by MAAP 4.

In addition to the parametric variation of the initial melt mass, the time of RPV failure is varied between 10000 s (3 hours) and 86400 s (1 day) to investigate the influence of the decay heat level in the MCCI pool on the failure time of the RPV-bottom and the retention time in the pit. This variation is equivalent to the assumption of different initiating scenarios, e.g. LBLOCA and SBLOCA. The resulting variation in the decay heat level is ~30%.

The principal tool for the assessment of the MCCI in the reactor pit is the computer code COSACO. To describe the configuration in the MCCI pool, the layer-model is used, which assumes the immiscible oxide and metal melts as stratified. The reasons for using stratified layers are:

- the high density difference of initially ~2000 kg/m³
- the expected formation of an oxidic crust at the oxide-metal interface as a result of the temperature of the metal melt being initially 550°C lower than that of the oxide

As a consequence, the downward MCCI is governed by the oxidic melt until its density finally falls below that of the metal melt due to the admixture of light concrete decomposition products into the oxide. This initiates a layer inversion, which relocates the metallic melt underneath the oxide and, at the same time, mixes the slag layer accumulated on top of the metal melt with the oxide. The slag layer consists of concrete eroded by the metal melt and of oxidation products formed within the metal melt.

In addition, calculations that assume a complete mixing of the oxidic and metallic melt phases throughout the retention period have been carried out.

2.4.2.1.2. Results

Melt accumulation is considered successful, if, for each analyzed case, the following targets are fulfilled, significantly before the MCCI pool contacts the melt gate:

- the MCCI in the pit is still ongoing at the time when the lower head plus lower support plate ("RPV-bottom") has failed and thus, the residual in-vessel melt is released into the pit and
- all incorporated material has been dissolved in the MCCI-pool and conditions that promote melt spreading are achieved

The compliance of the concept with these targets is demonstrated. The following results were obtained.

2.4.2.1.2.1. Melt accumulation

In all analyzed cases, the failure of the RPV-bottom occurs long before the melt front reaches the gate. This holds true, despite substantial deviations in the calculated total interaction time, caused by the variations in the decay heat level and the initial mass of melt in the pit. The initial amount of melt affects the duration of the temporary melt retention in so far, as an increased mass does not only result in a higher decay power, but also in a lower surface-to-volume ratio and thus in higher power densities at the melt-concrete interface and at the upper surface of the pool that faces the RPV lower head. The correspondingly higher thermal radiation from this surface accelerates the heat-up of the RPV-bottom.

It was found that the erosion progresses faster with the assumption of a stratified melt. Correspondingly, the mixed mode yields generally longer retention times. Despite this, the vertical erosion depth reached at the time when the RPV-bottom is calculated to fail is about the same for both assumptions. This confirms that, the RPV-bottom and the MCCI pool form a coherent system, so that achieving the ultimate lower head failure criterion and the second melt discharge are mainly a function of erosion depth rather than of erosion time. The criterion for failure of the RPV-bottom is achieved at an axial ablation depth between ~18 and 22 cm for all investigated cases. This range corresponds to masses of decomposed concrete of 30-40 Mg. Given a concrete decomposition enthalpy of 1730 kJ/kg, the energy spent to decompose these concrete masses varies between $5.2 \cdot 10^{10}$J and ~$7 \cdot 10^{10}$J. In total, the melt has to penetrate a concrete thickness of 50 cm to reach the gate, at which time it has typically eroded a concrete mass of 90-100 Mg.

This important result is a characteristic feature of the concept of temporary melt retention. It is attributed to the fact that the failure of the RPV-bottom takes place after it has absorbed a certain amount of energy, to be emitted from the melt by thermal radiation. The time needed to absorb this energy is governed by the radiant heat flux at the melt surface. For a low heat flux, as a consequence of a low decay heat level in the melt, the time to achieve the failure temperature of the RPV-bottom is correspondingly increased. At the same time, the heat flux into the concrete, which determines the ablation rate, is also lower. As the heat fluxes to the top and bottom in the gas-mixed molten pool are at least equal (but may be higher to the top), both heat fluxes change in roughly the same proportion. As a consequence, failure of the RPV-bottom always takes place at similar axial ablation depths independent of the actual level of decay heat.

The comparison of calculated release sequence obtained for the generalized melt release sequence with specific scenario-dependent release sequences, obtained with MAAP, shows the bounding character of the generalized melt release sequence, in particular for LBLOCA and LOOP scenarios. The melt release sequences obtained by MAAP for these scenarios are covered by each of the generalized melt release sequence analyzed in the parametric study independent of the assumption of mixing or layering of the metallic and oxidic phases during MCCI.

2.4.2.1.2.2. Corium conditioning

Regarding the second target, it was necessary to check whether the final characteristics of the melt at the end of the temporary retention phase are favourable with respect to the succeeding spreading process. This task comprises a comparison of the final values obtained for melt composition, liquidus temperature and melt temperature, as well as for the resulting volumetric solid fraction at the time of spreading. The latter is of importance, as it influences viscosity and thus the ability of the melt to spread.

The initial metallic U/Zr inventory is oxidized fairly early into the MCCI sequence. Even the discharge of fresh core melt at the time of the ultimate failure of the RPV-bottom does not result in a new accumulation in the melt. Any metallic U and Zr present in the initial melt will be completely oxidized before the end of retention.

Also, layer inversion takes place before the termination of the temporary melt retention in all considered cases. This leads to slag layer and oxidic melt mixing and, by this, strongly increases the concentration of concrete decomposition products in the oxidic melt, which further decreases its density and thus stabilizes the stratification.

During concrete admixture temperature of the oxidic melt was found to follow the evolution of the melt liquidus temperature which steadily decreased during the entire MCCI. In terms of the analyses conducted in the layered mode, the main event that disrupts this continuous decline is the second melt pour from the RPV, which causes a steep increase of the liquidus value. Despite substantial differences in the preceding course of the MCCI, the predicted liquidus temperatures at the end of temporary melt retention do fit into a narrow band.

The absolute temperature of the oxidic melt at the time of spreading was found to be in the order of 2000°C, as compared to the initial temperature of the melt as it is released from the RPV of about 2500°C. This temperature reduction of about 500°C is caused by the change in melt chemistry and by the admixture of concrete decomposition products. The lower temperature significantly reduces the radiant heat losses to the ambient during the spreading transient.

The calculated subcooling of the oxidic melt that is the temperature difference between liquidus and melt temperature is only some ten degrees at the end of the MCCI. In comparison to this, the temperature difference between the liquidus and the immobilization temperature of the melt, as characterized by a volumetric solid fraction of 0.5, is several hundred degrees. The resulting values of the volumetric solid fraction in the order of 0.05 yield correspondingly low viscosities of the oxidic melt and a good ability of the melt to spread after gate failure.

This holds true also for the mixed mode assumption despite the fact that here the volumetric solid fraction is initially high, due to the postulated addition and dispersion of "cold" metal in the oxidic melt. This introduces an additional delay before the start of the MCCI. In parallel with melt reheating the volumetric solid fraction steadily decreases. This process is only interrupted when a mixture of oxidic and metallic melt is added to the MCCI pool during the final failure of the RPV-bottom.

At the end of the MCCI the conditions in the mixed pool are very similar to the stratified case with the exception that the metallic fraction is now at the same high temperature as the oxidic fraction into which it is dispersed. The temperature of the oxide and its relevant volumetric solid fraction are practically identical to the stratified case, because it is in both cases determined by the similar amount of mixed-in concrete.

2.4.2.1.2.3. Mass and energy release during MCCI in the reactor pit

The prediction of mass and energy release during MCCI in the reactor pit uses initial and boundary conditions which yield conservative results regarding the containment response. The scenario chosen for this analysis is a surge-line break LBLOCA-scenario. It leads to vessel failure and melt release into the reactor pit at a very early point in time and thus involves a high decay power level in the melt.

At the same time, the melt release duration for this scenario is relatively short. Relative to other scenarios, it therefore yields high concrete ablation rates, which translate into conservative off-gas rates. The integral gas release is not much higher though, as it mainly depends on the eroded amount of concrete, which is determined by the position of the refractory shielding of the reactor pit, and by the (fixed) position of the gate. This amount is therefore almost independent of the scenario and corresponding melt release sequence.

The gas release temperature is assumed to correspond to the temperature of the particular melt that forms the upper layer of the MCCI pool. Hence, it corresponds to the temperature of the slag layer before layer inversion, and that of the oxide melt afterwards. As the oxide melt exhibits the highest temperature in the MCCI system, the release temperature increases after layer inversion. At the same time, the gas release rate strongly increases, due to the high transient ablation rates during contact of the concrete and superheated metal.

2.4.2.2. Validation of melt gate opening

2.4.2.2.1. Validation strategy

The design of the melt plug must ensure that, at the end of the period of temporary melt retention, a sufficiently large cross-section for the outflow of the melt will develop within a sufficiently short time. The latter is linked with the start of water overflow from the IRWST onto the melt, which is triggered passively by the arrival of the melt in the core catcher. The requirement is that this water should not interfere with the melt flow through the transfer and the melt spreading process within the core catcher. The analysis is required to demonstrate that this is ensured for any conditions that might be reasonably expected.

2.4.2.2.1.1. Contact modes

The composition and properties of the melt in the reactor pit at the moment of melt plug failure are defined by the final state of the MCCI in the reactor pit. These values are taken from the corresponding COSACO calculations for the MCCI in the pit. These calculations show that the total amount of concrete ablated and dissolved in the melt during the MCCI is almost independent of the severe accident scenario and of the vessel failure history.

Because the metallic and oxidic melt components are immiscible, a two phase melt configuration with separated metallic and oxidic phases is expected at the end of the MCCI. At the beginning of the MCCI in the reactor pit, the oxidic melt, with its high content in UO_2 and ZrO_2 has a higher density than the metal. Thus, the oxide layer will initially be located below the metallic melt. Lighter slag, mainly consisting of concrete oxides, accumulates on the surface of this metal layer.

With the ongoing dissolution of concrete at the bottom of the pool, the density of the oxidic phase steadily decreases and eventually approaches that of the metal. At that time the oxide and metal layers change position, which mixes the upper slag layer into the oxidic melt, and which further heavily reduces the oxide density. As a consequence, the initially three layer system is converted into a stable two layers with the metallic melt below the oxidic one.

This configuration, case A, is used as best estimate assumption for the analysis of temporary melt retention in the reactor pit. In all corresponding calculations the described layer inversion occurs before all concrete at the bottom of the pit is eroded. Therefore, the metallic melt is assumed to be the first to be released and spread.

Due to remaining uncertainties in the understanding of the MCCI in the pit, a partial mixing of the metal and oxide at their common interface due to the stirring effect of the uprising MCCI gases cannot be excluded. As a bounding case that covers the corresponding uncertainties, a complete mixing of the two melt phases is additionally considered in the analysis. In this mixed configuration, denoted as case B, homogeneous thermo-dynamic and thermo-chemical conditions are assumed in the underlying COSACO analysis.

In addition to these two configurations, which bound the spectrum of analytically predicted initial conditions, also the fictive case of a postulated “early” melt plug failure at the time before layer inversion is investigated. In this conservative case the oxidic melt is still located below the metal and slag, which corresponds to a three layer system, case C.

2.4.2.2.1.2. Size and location of the initial contact area

The size, shape and location of the initial contact area between melt and gate after penetration of the sacrificial concrete are impossible to predict, as they are determined by the uncertain course of the preceding MCCI.

However, the large diameter of the reactor pit and the fact that the surface of the gate is less than a tenth of the total surface of the pit bottom give rise to the expectation that the concrete ablation, across the scale of the gate, will be practically homogeneous and the erosion front correspondingly flat. As a consequence, a large region of the gate, if not the entire gate, would get in contact with the melt within a short period of time, which automatically results in the required fast opening of a large cross-section. Therefore the expected initial conditions require no further analysis.

To show that the gate opening is insensitive to this assumption of homogeneous erosion, the case of a postulated local contact was analysed. Corresponding initial contact sizes are estimated from available large-scale MCCI experiments. These values are to be seen as a conservative estimate due to the limited size of these experiments and other test-specific restrictions. Two bounding cases of the contact location were considered: a central position and a position in the extreme corner of the melt plug where hole enlargement is restricted on two sides by the presence of the surrounding zirconia layer.

2.4.2.2.1.3. Hole enlargement during melt outflow

After local penetration of the sacrificial concrete and thermal failure of the aluminium gate the melt pours into the transfer channel and from there into the core catcher. The heat flux from the out-flowing melt to the concrete around the initial opening as well as the ongoing MCCI at the top of the residual concrete cause a steady increase of the open cross section. The aluminium gate underneath is not of relevance as it is quickly destroyed during melt contact.

The value of the heat flux from the bulk of the flowing melt to the concrete is considered to be proportional to the driving temperature difference and the to effective heat transfer coefficient between bulk and concrete interface. To determine values for these parameters, a combination of empirical and phenomenological models is used which are based on appropriate experimental results.

Because the thermal conductivity of the concrete is very low, heat conduction into the concrete behind the erosion front can be neglected. Therefore the obtained heat flux is fully translated into a corresponding erosion rate that can be determined using the known values of concrete density and decomposition enthalpy.

2.4.2.2.2. Obtained results

For the expected case of a quasi-instantaneous opening of the gate with large cross-section the obtained total melt release time is in the order of one minute. Longer times are obtained for the postulated case of a local initial contact and with the deduced minimum cross-section. For this latter case with an assumption of a constant hole size, outflow times would be in the order of 5 to 10 min. When considering hole enlargement during melt outflow these times are drastically reduced.

The shortest times are obtained for the best-estimate case A, characterized by metal being the first phase released. Here the total outflow times are all very short, and practically independent from the initial hole size and position. Cases B and C yield longer time and show a more pronounced dependence on initial size and position. Nevertheless, for all these cases release times of less than 200 s are achieved.

2.4.2.3. Validation of corium spreading

After penetrating the melt plug the accumulated corium which amounts to a predicted mass of about 400 Mg (about 60-70 m³) pours through the melt discharge channel into the lateral core catcher. At its outlet, the melt enters the core catcher at a level more than half a meter above the bottom. The inflowing melt is guided over a concrete ramp designed to avoid local penetration of the sacrificial concrete near the entrance position and then distributes on the provided area of 170 m². Dry conditions are ensured by the fact that the spreading compartment is, by design, a dead-end room isolated from the rest of the containment. There is no possibility of a direct inflow of water from sprays or leaks. Only a limited amount of condensate can be formed at the walls inside the spreading room itself.

Due to the elevated inflow position, the initial spreading process on the concrete floor will turn into a “fill-up” of the core catcher as soon as a sufficient melt depth is reached. From that time on, the melt no longer needs to distribute on the surface, but the melt level in the core catcher rises almost uniformly across the entire melt-covered area.

2.4.2.3.1. Validation strategy

To justify the effectiveness of the melt spreading and distribution process for the EPR, several diverse approaches are applied. They include common CFD-based spreading models, like the code CORFLOW as well as phenomenological models, like the approach developed at RIT Stockholm. They are all validated against the large existing experimental data base.

2.4.2.3.1.1. Spreading analysis using the CORFLOW computer code

Several CORFLOW spreading calculations were performed with different assumptions regarding the configuration of the molten pool in the pit, which is either stratified or mixed. All considered cases led to an almost homogeneous distribution and an equal layer thickness of the corium in the spreading compartment after a period of less than a minute.

Considering the good results of the CORFLOW simulation for various experiments, including the 2D-spreading test COMAS EU-4 with prototypic, initially layered oxide and metal phases, it is concluded that the EPR spreading process can be represented with reasonable accuracy by the single component fluid modelling assuming an emulsion, with the metal phase mixed into the oxide. For this reference spreading case, variations of the major assumptions have been investigated which include the separate and subsequent spreading of the metallic and oxidic phases. For all analysed cases a complete coverage of the spreading area was obtained. The spreading process is almost synchronous with the melt release from the pit.

Comparative calculations with a finer horizontal spatial numerical mesh, performed for metallic, oxidic and mixed corium spreading, showed the low sensitivity of the results on this modelling assumption.

2.4.2.3.1.2. Analysis of corium spreading using the RIT approach

2.4.2.3.1.2.1 Objective

The main target of melt accumulation in the reactor pit is to achieve a one-step release, with relatively high melt flow rate and sufficient melt "superheat" relative to the immobilization temperature of the corium-concrete mixture. The total mass of metal and oxide melts is in the range of 400 Mg (about 60-70 m³).

The objective of the work summarized in this chapter was to apply the phenomenology-based methodology for the evaluation of melt spreading, developed at the RIT Stockholm **Error! Reference source not found.** to the characteristics of the EPR spreading situation. The RIT method is not based on the use of codes involving numerical solution of the Navier-Stokes equations. It can therefore provide a diverse validation of spreadability.

According to the RIT model, which is verified by post- and pre-calculations of various experiments, the most important parameter for the spreading process is the final thickness of the spread melt and not the dynamics of the spreading process.

2.4.2.3.1.2.2 Experimental evidence on spreading

A number of experiments have been performed to study the phenomenology of core melt spreading on the containment floor. The main objective of these experiments was to provide data and observations for model development and validation. In particular, experimental programs conducted at JRC (FARO L-26), SNU (COMAS), RIT (S3E), CEA (VULCANO) and FZK (KATS) are directly related to the verification of the EPR melt retention scheme. Despite partial non-prototypic characteristics, like small scales, low temperatures, simulant materials, spreading channel geometry, these experiments provided valuable insights into the physics of core melt spreading.

In the KATS experiments, e.g. it was observed that even though the various (uncoated, coated, dry, wet) concrete spreading surfaces are somewhat different from that of ceramic, the spreading length is comparable. In addition, the presence of shallow water was found to have no detectable influence on spreading for high pour-rate melt discharges. In the COMAS experiments, it was observed that the spreading distances were similar in channels with steel, ceramic and concrete substrate. In FARO L-26 even native oxidic corium was found to spread very well despite a low melt superheat. For COMAS 5a spreading was even successful at melt temperatures deep in the solidus-liquidus range.

2.4.2.3.1.2.3 Description of the methodology

In general, melt spreading is a complex, thermo-fluid process, which is governed by

(1) the hydrodynamic motions of the spreading liquid (melt), and

(2) the solidification of melt during the spreading process.

Item (1) is affected by gravitational, inertial, viscous and surface forces. Depending on the viscosity, the liquid spreading may be categorized into gravity-inertia and gravity-viscous regimes. Item (2) is affected by heat transfer from core melt to surrounding media, i.e. downward: q''_{dn} and upward: q''_{up} heat removal rates, decay heat generation rate q_v , and phase changes of the melt. For the EPR melt retention conditions, other phenomena (e.g., molten corium-coolant and molten corium-concrete interactions, melt stratification) are found to have negligible effect during the short time period of spreading, or they have been shown to be bounded by other phenomenological and scenario uncertainties.

An in-depth review of the state-of-the-art knowledge of melt spreading (database, simulation, analysis methods and scaling considerations) was performed in [11], which also gives a complete description of the RIT methodology. This methodology was first developed for spreading in one-dimensional channels, but has recently been extended to also cover spreading in 2D-channels and, more importantly, for spreading into open area.

In the RIT method, the terminal spread melt thickness δ_{spr} is shown to be a function of the time scales of two competing processes: hydrodynamic (convective) spreading τ_{conv}, and solidification τ_{sold}. In the gravity-inertia regime, the hydrodynamic spreading time scale τ_{conv}, is determined as the time period required for liquid (melt) to reach its capillary thickness, δ_{cap}. The characteristic solidification time, τ_{sold} , is defined as the time period needed to cool the melt to an immovable state. For this, not only the superheat, but also a part η of the latent heat of fusion, has to be removed from the bulk melt. Based on the mass and momentum conservation equations, a square-root relation was established between the dimensionless length scale (representing ratio δ_{spr} /δ_{cap}) and the dimensionless time scale (representing ratio τ_{conv} /τ_{sold}). The square-root law was shown to be valid in both gravity-inertia and gravity-viscous regimes, employing a dimensionless viscosity number, which was analytically derived.

2.4.2.3.1.2.4 Methodology validation

An experimental program named: "Scaled Simulant Spreading Experiments" (S3E) was performed at RIT. The S3E data were analyzed and found to fit very well with the scaling rationale developed. The RIT method was then used to predict the spreading distance in one-dimensional high-temperature oxidic melt spreading tests at RIT. Very good agreement between the pre-test prediction results and data was obtained. The validation success confirmed assumptions made in deriving the model equations (e.g., η= 0.5) and justified the use of the heat transfer correlations employed.

Extensive validation of the RIT method was performed against experimental data from KATS, COMAS, VULCANO and FARO spreading experiments. The method was found to predict, with reasonable accuracy, the spreading distance in one- and two-dimensional channels (COMAS EU-4, VULCANO and FARO L-26). It was also found that the spreading in two-dimensional channels is bound by the channel's sidewalls and hence essentially one-dimensional.

The RIT method was employed to perform pre-test predictions for COMAS EU-2b core melt spreading experiment with good agreement between the predicted and observed spreading distance.

Validation of the RIT method for melt spreading into open area was also performed on the data base obtained from the RIT simulant-material experiments. It was found that melt spreading into an open area is significantly different from the one-dimensional spreading. As melt spreads in all directions, the hydrodynamic spreading time scale is remarkably reduced, and hence the spreading area is significantly enhanced. As a result, the spread melt thickness in the open-area spreading case may decrease by a factor of 3 to 10, as compared to one-dimensional spreading.

2.4.2.3.1.2.5 Application to the EPR spreading case

The methodology developed at RIT was employed to predict the core melt spreading characteristics for the EPR case. The actual design of the EPR spreading room corresponds to a spreading into an open area, both RIT methods for (i) an open area and (ii) a channel were employed. The latter represents the conservative lower bound estimate for the melt-covered area.

The characteristics of core melt spreading in the EPR case were evaluated for selected core melt accident scenarios, in which melt superheat and melt flow rate as well as melt physical properties are subject to uncertainties. The effect of both the scenario and the phenomenological (modelling) uncertainties are delineated. A probabilistic assessment framework, incorporating the deterministic and parametric models, was developed to propagate both phenomenological and scenario uncertainties in the evaluation of the safety-important parameters, i.e. the terminal spread-melt thickness, or the coverage of the melt retention area by core melt. Such treatment of uncertainties achieves an integrated assessment, showing the influence of different uncertain parameters on the results obtained.

The assessment was performed for two basic cases, with low (case A) and high (case B) amount of sacrificial concrete slag added to the oxidic corium before spreading. Again, only the oxidic melt fraction was considered. In addition, a lower range of core melt discharge rate was chosen for a bounding evaluation of the spreading characteristics for case B.

In all selected cases, it was found that even the one-dimensional spreading model predicts nearly complete spreading (A_{theo}/A_{EPR} = 0.85..1). In comparison, the spreading-into-open-area model predicts a ratio of A_{theo}/A_{EPR} >> 1. The higher ratio in the 2D-case is due to the fact that, even if melt becomes locally immobilized, such obstacles can be passed-by, without restrictions introduced by channel sidewalls.

Results of the sensitivity analysis indicate that the important parameters are: total melt mass and melt discharge rate. Within the range of these parameters investigated, other influences, like scenario and phenomenological uncertainties were found to have no profound impact on the results of the assessment.

To summarize; the results of the assessment of core melt spreading in the EPR melt retention device show that for the given melt delivery conditions the entire spreading area will be covered uniformly.

2.4.2.4. Analysis of the corium/concrete interaction in the spreading area

2.4.2.4.1. Validation strategy

For the analysis of the MCCI in the core catcher the surge-line break scenario is used. Relative to other scenarios, this scenario yields a high decay power in the melt. It therefore yields the highest erosion rates and is thus conservative with respect to the earliest time of melt contact with the cooling structure.

In addition, the layered mode is used to model the MCCI pool configuration, which in terms of the MCCI in the core catcher assumes the metallic layer to be located underneath the oxidic layer throughout the entire MCCI. Combination of both assumptions yields highest ablation rates, which result in a low duration of the MCCI and at the same time translate into high gas release rates. The integral gas production is independent of the molten pool configuration as it is determined by the given amount of ablatable concrete.

In terms of consistency, the analysis employs the particular melt conditions predicted for such a scenario at the end of the MCCI phase in the pit as melt initial conditions.

For the heat transfer at the free surface of the melt, for both, the phase before and after flooding, radiant heat transfer to the ceiling of the spreading compartment is considered. The start of flooding after about 5 min is not considered due to the limitations of the model. Therefore, the determination of gas release from the MCCI is decoupled from the evaluation of the steam production resulting from the flooding of the melt free surface.

The MCCI terminates when the concrete layer is completely ablated. The analysis of the MCCI in the core catcher is performed with the MCCI computer code COSACO.

2.4.2.4.2. Obtained results

2.4.2.4.2.1. Ablation front progression and temperature evolution

In consistence with the layered melt assumption, only the metallic phase interacts with the concrete on the horizontal cooling structure. As the metallic melt is initially superheated, the ablation behaviour is characterised by two subsequent, distinctly different phases.

The first phase is characterised by the transient cool-down of the metallic melt which goes along with high ablation rates. This phase prevails until the metallic melt has cooled down to its freezing temperature. During the second phase, ablation front progression is quasi-steady and practically proportional to the combined decay heat generated in the oxide and metal melt. The temperature of the metallic melt remains almost constant at its freezing temperature. The cooling structure is reached after several minutes to half an hour, depending on the local concrete thickness.

In comparison the time to flood the bottom part of cooling structure is far below 100 s. This shows that high margins exist. In addition, the fact that the metallic melt cools down to the freezing temperature and forms crusts at the bottom reduces the thermal loads on the cooling structure during initial contact, thus yielding a soft transient thermal response.

2.4.2.4.2.2. Gas release in the containment due to MCCI in the core catcher

The initial, transient phase is characterized by high ablation rates and accordingly by high gas release rates and contrasts to the following quasi-steady phase, during which the release rates are about one order of magnitude lower. The gases released are H_2O, H_2, CO_2 and CO. The release temperature of the gases is assumed to be equal to the temperature of the particular melt which forms the upper layer of the MCCI pool. In terms of the MCCI in the core catcher, the release temperature is thus the temperature of the oxide melt.

2.4.2.5. Analysis of corium flooding and quenching

2.4.2.5.1. Main phenomena

Water will pour onto the surface of the spread melt after the start of overflow from the sidewall structure. The quench-front will then move on the melt free surface from the periphery to the centre of the core catcher.

At that time, the MCCI is still ongoing and the hot melt is subject of an intense convective mixing, driven by concrete decomposition gases. This causes a steady transport of hot melt to the surface and a high convective heat flux at the interface with the water. As a result, the surface temperature remains high so that film boiling is the dominant heat transfer mode. In the film boiling regime an efficient heat transfer is anticipated owing to conduction and radiation across the agitated (i.e. area enhanced) melt-water interface. In addition, melt droplets will be entrained into the overlaying water.

Shortly after, the melt enters a transient bulk-freezing phase. Since solid oxidic corium has a higher density than the liquid, fragments of frozen material (formed at the surface) will be re-mixed into the molten pool and will cause an overall decrease in temperature. This process leads to a collapse of the gas-film and eventually to the formation of a slurry-type, viscous oxidic melt. The drop in surface temperature, which results from the switch to gas-enhanced, nucleate boiling is accompanied by the formation of a crust.

The late bulk-freezing phase is characterized by a strong decline in superficial heat-flux to almost zero. In this state the melt becomes thermally "insulated" from the water. As a consequence, the bulk temperature starts to rise again (due to decay heating) and convection re-establishes. The temperature of the melt and the thickness of the crust then approach their steady-state value which is influenced by the level of internal decay heat generation.

The forming crust can provide support for melt particles and droplets that are drained into the water by the flow of concrete decomposition gas through cracks and holes in the crust. Corresponding melt ejections through volcano-like structures have been observed in experiments with simulant and prototypic material. The created particle bed transfers its internal decay heat directly to the water. An effective cooling is also achieved within porous regions of the crust that are potentially created during thermal cracking. The relevance of this process is, however, subject to ongoing R&D and can therefore not be reliably evaluated. In all EPR studies a best-estimate value for the coolable melt fraction of 20 wt% has been assumed.

Locally, the described stages of the quenching process will occur in a sequential order. However, because the water is provided only at the circumference the central region will be flooded last. Various stages of melt-water interaction will therefore coexist at different locations at the same time.

2.4.2.5.2. Validation strategy

Based on above-described phenomenology the following assumptions are made to determine the heat transfer during the individual phases of quenching.

2.4.2.5.2.1. Initial flooding of the corium

This phase covers the period between the first pouring of water onto the melt and the complete flooding of the entire surface. It is assumed that, during this phase, the total heat transport from the bulk of the melt to the surface exceeds the power needed for all added water to be vaporised. Therefore, the rate of steam generation corresponds to the flooding rate.

The duration of the flooding period dominantly depends on the assumption, which fraction of the energy initially stored in the melt can be released to the water. The two mechanisms that provide the energy during this phase are: bulk cooling and superficial fragmentation. Therefore, the parameters that determine these two processes also determine the duration of the flooding phase and thus the steam and energy release into the containment. These are the degree of superficial fragmentation, and the values for the temperature drop related to bulk cooling and quenching

This first phase ends when the initially available heat plus all decay heat generated during this period is consumed to transfer the incoming water into steam. The corresponding time can be obtained by solving the related energy balance.

For the quenching process only the upper, oxidic part of the melt is considered. This is justified because, following the preceding MCCI, the temperature of the metallic melt is always lower than that of the oxide, so no energy can be transferred from the metal to the oxide. Therefore neglecting the metal is conservative, as in reality, it will serve as an additional heat sink for the oxide.

2.4.2.5.2.2. Water fill-up phase

After the end of the initial flooding period, the rate of steam generation will fall short of the flooding rate, so water can start to accumulate atop the melt pool. At that time the pool effectively consists of a fragmented oxide layer and a bulk part below, which is at relatively low temperature. The water inflow rate remains almost constant as it is mainly defined by the fixed height of the circumferential overflow. The level decrease in the IRWST itself is negligible.

The decay power released within the fragmented part is directly transferred to the water, while the decay power in the bulk will be used to re-heat the melt. During the bulk re-heating period only the fragmented melt fraction transfers energy to the incoming water. This energy equals the decay power in the fragmented region. For low values of the assumed degree of fragmentation this power is not sufficient to lift the incoming water up to saturation temperature. In this case the accumulating water pool atop the melt will be subcooled and steaming into the containment is completely stopped.

It is assumed that, after the melt is again at a sufficiently high temperature all decay power generated in the bulk of the oxidic melt will be available for the heat-up of the water. This power is typically sufficient not only to saturate the incoming water but, after some time, also the already accumulated subcooled water atop the melt. As soon as this inventory is saturated, steaming into the containment restarts.

2.4.2.5.3. Obtained Results

According to the models described in the previous chapter, the course of steam release into the containment is calculated in a conservative way.

It displays an initial period of maximum steam release into the containment, all the incoming water being vaporised, which duration is in the order of half an hour. After this, steaming stops over a long period of several hours (depending on the assumed number of open valves) and then restarts with a rate that corresponds to the actual decay power.

2.4.2.6. Analysis of long term corium stabilization

The end of the MCCI in the core catcher determines the time of initial melt contact with the cooling plate. By comparing the calculated duration of the MCCI with the time needed to completely flood the melt with the design base flooding rate, it is obvious that the melt will be completely flooded at that time and therefore fully enclosed within water or water-cooled surfaces. The corresponding heat fluxes to the side, top and bottom must be safely absorbed.

2.4.2.6.1. Validation strategy

For validating the function of the core catcher a number of diverse approaches are applied. They include generally bounding assessments based on empirical and phenomenological models, as well as the application of the computer code WALTER, to determine transient behaviour of the cooling structure after melt contact, and the long-term temperature profiles inside the melt.

2.4.2.6.1.1. Bounding steady state heat fluxes

A conservative value for the steady-state heat flux to the cooling structure and the overlaying water can be obtained by assuming that all decay heat must exclusively be carried into the water pool atop the melt. The thus obtained heat flux also provides a bounding estimate for the cooled sidewall because the heat flux to the side can, in average, not be higher than that to the top, due to the fact that the main heat transport mechanism is natural convection.

Given a total decay power in the order of 25 MW and a top/bottom area (after MCCI) of 180 m² the resulting value is <150 kW/m². This low value illustrates that the heat transfer to the top and sides does not constitute a problem, the related CHF[2] limits being much higher with comfortable margins.

A similar method can be used to derive a bounding heat flux into the bottom cooling plate. The corresponding model is to assume that the heat fluxes to all surrounding surfaces (top, bottom and sides) are the same. Such an isotropic distribution does not exist under natural convection conditions, because the heat flux to the bottom is always significantly lower than to the top, which justifies the bounding character of the obtained value.

With a melt-sidewall contact area of about 25 m², the related bounding value for the steady-state downward heat flux is 25 MW/ (2*180m² + 25m²) = 65 kW/m².

2.4.2.6.1.2. Transient heat fluxes

During the initial contact between melt and cooling plate the resulting transient thermal loads can in principle be higher than their steady-state values. To analyse this situation, corium and cooling plate were modelled using the code WALTER. This computer code allows the simulation of 1D heat conduction/convection processes with solidification in stratified layers and is thus suited to assess the problem. The parameters that determine the heat transfer within the system were chosen as follows:

Heat transfer between corium and cooling plate

Based on the fact that:

- the preceding MCCI creates a pre-existing metallic crust at the interface between the metallic melt and the “cold” concrete

- general foundry experience [19] as well as the analysis of a large scale COMAS spreading experiments show that even superheated iron melts form crusts when poured onto “cold” metal surfaces

it is assumed that a gap exists between the melt and the cooling structure. Gap formation is generally explained to result from the shrinking of the molten steel during solidification on a cold wall. It reduces the contact area to a few spots that support the mechanical load. Heat transport across the gap is predominantly by thermal radiation enhanced by convection and local conduction, considered by a combined heat transfer coefficient.

[2] CHF: Critical Heat Flux

Heat transfer between the cooling plate and water

From corresponding experiments it is known that the entire inner surface of the channel, including its top, will stay in contact with water as long as the heat flux from the top remains below a value of 60-80 kW/m² (at 1 bar). For greater heat fluxes the upper region of the channel will dry out and heat will be transported mainly through the sidewalls. With increasing heat flux, the steam content in the channel increases and the region of heat transfer moved downwards.

As moving heat transfer boundaries cannot be modelled in the code, a fixed wetted height of 80% of the total height of the cooling channel is assumed throughout the calculation. This corresponds to the experimentally observed situation at a heat flux of about 100 kW/m² (1 bar). The upper 20% of the channel walls and its top are considered adiabatic. The chosen simplification artificially decreases the heat transfer to the water. This results in higher temperatures of the cooling plate and hence is conservative with respect to the validation of the cooling function.

2.4.2.6.2. Results

Several calculations were performed for the bottom structure varying initial melt conditions and main parameters, including the initial temperature and thickness of the metal and oxide layers. The performed calculations show that the cool-down process can be separated into an initial transient phase which reveals relatively high heat fluxes (this transient phase is exclusively driven by the cool-down of the metallic layer), and a phase characterised by quasi-steady conditions with heat fluxes decreasing with the decay heat.

The obtained heat flux peak values for both regimes are significantly lower than the CHF limits experimentally observed for the bottom cooling structure in a 1:1 mock-up [23], which confirms that the core catcher can fulfil its function under the expected thermal loads. The fact that during a severe accident the containment pressure will be significantly higher than the experimental value of 1 bar further increases the cooling capability of the core catcher, and the corresponding margins for the downward heat transfer.

LIST OF REFERENCES

[1] Sehgal, B.R.et al 'Final Report for the "Melt-Vessel Interactions (MVI)" Project', SKI Report 00:53, Dec. 2000

[2] W. Steinwarz, et al. 'Experimental Investigations on Corium Interaction with Refractory and Sacrificial Layers (CORESA') - BMWI project 1501212, Final Report. Siempelkamp Nukleartechnik GmbH, SNT-AB-2002-01

[3] M.T. Farmer, et al. *'MACE Test M3b, Data Report',* MACE-TR-D13, Vol. 1/2; Argonne Nat. Lab., Nov. 1997

[4] W. Steinwarz, et al. 'Investigations on the Phenomenology of Ex-vessel Core Melt Behaviour'
Final report, EU 4th FWP, EXV-COMAS(99)-D27

[5] Urbain, G. '*Viscosity Estimation of Slags*', Steel Research Vol. 58., pp. 111-116, 1987

[6] Thomas, D.G. 'Transport Characteristics of Suspensions: VIII. A Note on the Viscosity of Newtonian Suspensions of uniform spherical Particles', Journal of Colloid Science, Vol. 20, pp. 267-277, 1965

[7] Stedman, S.J., Evans, J.R.G., Woodthorpe, J. 'Rheology of composite ceramic injection moulding suspensions', Journal of Material Science, 25, pp. 1833-1841, 1990

[8] Ramaciotti, M., 'Étude du Comportment Rhéologique de Mélanges issus de l'Interaction Corium/Béton (Study of the Rheological Behaviour of Mixtures emerging from the Corium/Concrete Interaction)' Doctoral Thesis from Provence University(Aix-Marseille I), 24. September 1999

[9] Farmer, M.T., Spencer, B.W., Aeschlimann, R.W. *'Liquidus/Solidus and Zr Solubility Measurements for PWR and BWR Core Melt Compositions'* Proceedings of the OECD Workshop on Ex-Vessel Debris Coolability, Karlsruhe, Germany, 15-18 November, 1999, FZKA 6475

[10] M. Eddi, G. Bandini 'Preliminary analysis on corium spreading in reactor core-catcher with THEMA code' SAM-ECOSTAR-P07-17/01, Feb. 2002

[11] B.R. Sehgal, T.N. Dinh, R.R. Nourgaliev, M.J. Konovalikhin, V.A. Bui *'Assessment of Core Melt Spreading in EPR Melt Retention Device'.*Sehgal Associates Inc., October 15, 1998

[12] Farmer, M.T. et al. *'MACE Test M1B - Data Report',* ACE-TR-D6, Argonne Nat. Lab., Sept. 1992

[13] M.T. Farmer, et al. *'MACE Test M4, Data Report',* MACE-TR-D16; Argonne Nat. Lab., Aug. 1999

[14] B. Eppinger, F. Fellmoser, G. Fieg, H. Massier, G. Stern 'Experiments on Concrete Erosion by a Corium Melt in the EPR Cavity: KAPOOL 6-8' Forschungszentrum Karlsruhe, March 2000, FZKA 6453

[15] B. Eppinger et al 'Simulationsexperimente zum Ausbreitungsverhalten von Kernschmelze: KAPOOL 8-17' Forschungszentrum Karlsruhe, March 2001, FZKA 6589

[16] J.-M. Seiler et al 'European Group for Analysis of Corium Recovery Concepts – EUROCORE' Synthesis report, presented at FISA 2001, Luxembourg, Nov 12-14

[17] Farmer, M.T. 'Comments on SSWICS Test Results' Presented at 3rd OECD-MCCI Program Review Meeting, Garching, Germany, May 2003

[18] J.M. Seiler, K. Froment 'Material Effects on Multiphase Phenomena in Late Phases of Severe Accidents of Nuclear Reactors', Multiphase Science and Technology Vol 12, Nr 2 p 117-257, 2000

[19] A.G. Gerber, A.C. Sousa 'Numerical Investigations of the Influence of Air Gaps Upon the Solidification in a Rotary Caster', Journal of Materials Processing Technology 48 (1995), p. 657-665

[20] Rouge S., Dor I., Greffraye G. *'Reactor Vessel External cooling for Corium Retention SULTAN Experimental Program and Modeling with CATHARE Code'*, OECD Workshop on In-Vessel debris retention and coolability, Garching, Germany, 3-6 March 1998

[21] O. Kymäläinen, et al 'COPO - Experiments on heat transfer from a volumetrically heated pool' IMATRAN VOIMA OY, DLV1-G380-0377, April 1993

[22] Sehgal, B.R., Nourgaliev, R.R., Dinh, T.N. 'Characterization of heat transfer processes in a melt pool convection and creep experiment' Proceedings of NURETH-9, San Francisco, CA, U.S.A., October 1999

[23] Fischer M., O. Herbst, H. Schmidt 'Demonstration of the heat removing capabilities of the EPR core catcher' 3rd International symposium on two-phase flow modelling and experimentation, Pisa, Italy, September 22-24, 2004

[24] H. Alsmeyer, W. Tromm 'The COMET Concept for Cooling Core Melts: Evaluation of the Experimental Studies and Use in the EPR', EU report: EXV-CSC(99)-D036 FZK 1999

[25] L. Meyer, M. Gargallo 'Low pressure Corium Dispersion Experiments with Simulant Fluids in a Scaled Annular Cavity', 2003, Nuclear Technology, 141, pp. 257-274

[26] H. Alsmeyer et al. 'Ex-vessel core-melt stabilization research (ECOSTAR)', Proceedings of FISA 2003, Luxembourg, Nov. 2003

S.2.2.4 FIG 1 : PRINCIPAL STRUCTURES IN THE EPR CONCEPT OF CORIUM RETENTION

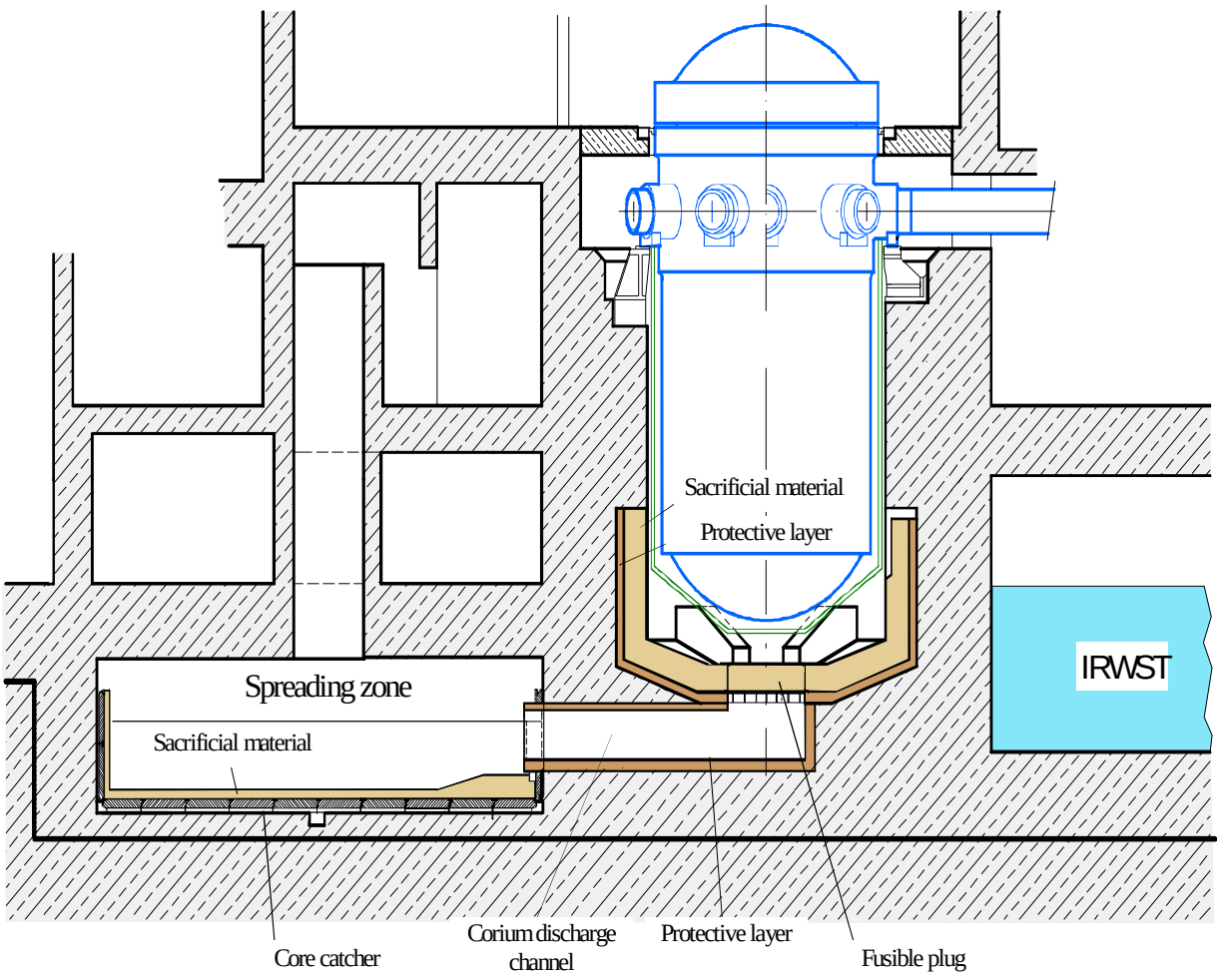

S.2.2.4 FIG 2: MODELLING DIAGRAM APPLIED TO THE GENERAL SEQUENCE OF POURING THE CORIUM FROM THE REACTOR VESSEL

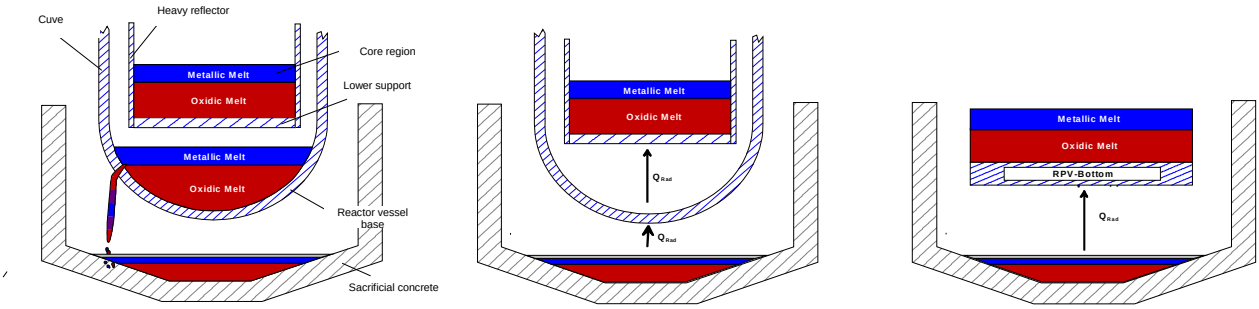

(a) **(b)** **(c)**

S.2.2.4 FIG 3: DIAGRAM REPRESENTING THE SITUATION DURING PASSIVE COOLING OF THE CORIUM. THE WATER LEVELS AT EQUILIBRIUM IN THE REACTOR PIT AND IN THE SPREADING AREA FOLLOWING THE GRAVITY-DRIVEN FLOW OF WATER FROM THE IRWST.

(The figure is not realistic with respect to the sacrificial layer, which is already eroded at this time)